Multi-Material Design and Performance Analysis of Pneumatic Soft Actuators

UDC:007.52:531.1
Original scientific paper https://doi.org/10.46793/aeletters.2026.11.2.5

Barnabás Piri[1], Szabolcs Berezvai[1*]

[1]Department of Applied Mechanics, Faculty of Mechanical Engineering, Budapest University of Technology and Economics, Műegyetem rkp. 3, H-1111 Budapest, Hungary

Abstract:
Soft robotics has emerged as a promising and rapidly evolving field, replacing traditional rigid systems with highly compliant elastomer actuators that offer adaptable interactions with their surroundings. Driven by cost-effective fabrication techniques like molding, 3D-printing, and laser cutting, these systems frequently utilize pneumatic actuators to mimic biological muscle behavior. However, optimizing these designs remains difficult due to the highly nonlinear mechanical behavior of rubber-like materials and the complex fluid-structure interactions that occur during pneumatic actuation. To address these challenges, the primary aim of this research is to analyze the mechanical behavior of laser-cut, pneumatically actuated multi-material soft robotic structures. To achieve this, finite element (FE) simulations, validated against experimental measurements, were used to evaluate how different geometries and material compositions respond to actuation. By systematically examining these mechanical responses, this research aims to contribute to a broader understanding of how soft robots can be deployed more effectively and widely in the future. The main results showed that the triangular actuator shape is optimal for low-pressure, high-precision applications, whereas the rectangular and elliptical actuators can generate high grasping forces. The results also highlight the importance of the internal design of the actuator, showing that increased chamber density enhances bending in certain shapes while causing localized distortions in others.

ARTICLE HISTORY
Received: 30 April 2026
Revised: 18 June 2026
Accepted: 24 June 2026
Published: 29 June 2026

KEYWORDS
Soft-robotics, Pneumatic actuators, Hyperelasticity, Finite element method, Experimental testing

1. INTRODUCTION

Traditional robotic systems are typically constructed from rigid links and discrete joints, enabling high precision, repeatability, and load-bearing capacity. However, these systems are inherently limited when operating in unstructured environments or in applications requiring safe interaction with delicate objects or humans. Their rigid architecture restricts adaptability and often necessitates complex sensing and control strategies to handle uncertainty [1-3]. In contrast, soft robotic systems employ highly compliant materials, such as elastomers, hydrogels, and other soft solids, allowing continuous deformation and inherently safer interactions. This paradigm shift enables robots to achieve biologically inspired motion and passive adaptability, making them particularly suitable for tasks where conventional rigid robots are less effective [4-6]. Recent advances have established soft robotics as a rapidly growing field, with significant developments in design [7], fabrication [8], and control methodologies [9-11].

Soft robotic systems can be categorized based on their actuation principles. Among these, fluid-driven actuators (eg. pneumatic systems) represent one of the most widely adopted approaches due to their structural simplicity, large achievable deformations, and ease of fabrication. Other actuation methods include hydraulic systems,

*CONTACT: Szabolcs Berezvai, e-mail: berezvai@mm.bme.hu

tendon-driven mechanisms, electroactive polymers, shape memory materials, and magnetically responsive structures [12-14]. Each approach offers distinct advantages and limitations in terms of controllability, response time, and achievable force output. Nevertheless, pneumatic actuation remains dominant in many applications, despite introducing complex fluid-structure interactions and strongly nonlinear mechanical behavior that complicate modeling and design optimization [2].

The operation of soft grippers is typically based on deformation mechanisms induced by internal pressurization. These structures consist of chambers embedded within a highly compliant body that expand under internal pressure, generating asymmetric strain distributions that result in controlled bending motion. The mechanical response of soft actuators is governed by a complex interplay between geometry, material properties, and loading conditions [11, 15, 16]. The highly nonlinear, finite-strain behaviour of rubber-like materials, often described using hyperelastic constitutive models, further complicates predictive modeling and necessitates the use of advanced numerical methods.

Despite significant progress in the field, the systematic investigation of how geometric design parameters and material composition influence the mechanical response of pneumatically actuated soft structures remains an open challenge. In particular, the combined effects of actuator geometry, internal chamber configuration, and material selection on deformation behavior are not yet fully understood.

In this research, the mechanical behavior of laser-cut, pneumatically actuated soft robotic structures is investigated through a combined experimental and numerical approach. The actuators are inspired by the *Pneu-net Bending Actuators* [17].

In this research, multiple actuator geometries and chamber configurations, along with different silicone materials, are considered to evaluate their influence on deformation characteristics. Finite element simulations are performed to capture the nonlinear response of the structures, and the results are validated through experimental measurements. The findings contribute to a deeper understanding of the design parameters governing soft actuator performance and support the development of more efficient and adaptable soft robotic systems [18].

2. MATERIALS AND METHODS

This section summarizes the methods used in this work, starting with the specimen fabrication. The material characterization was performed by uniaxial tensile and compression tests. The numerical simulations were performed in *ABAQUS* [19], while the experimental validation was carried out using a self-developed fluidic control board, accompanied by a set of video recording equipment.

2.1. Specimen Fabrication

The soft actuators applied in this study consist of two main parts. The bottom layer is a solid base, made from *ELASTOSIL 4601 A/B* silicone (Shore A 28) [20], while the top layer is made from *ECOFLEX 00-30* or *ECOFLEX 00-50* (Shore 00-30 and 00-50, respectively) [21], shown in Fig. 1. The top layer contains chambers that expand during internal pressurization, causing the actuator to bend. The two layers are molded separately and glued together with a silicone adhesive.

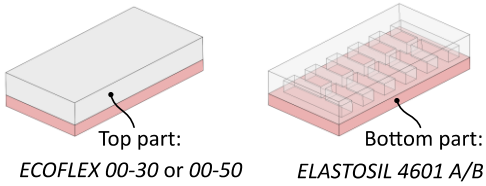

Fig. 1. The two main parts of the soft actuator

In this research, three main types of actuators were analysed: rectangular (*R*), triangular (*T*) and elliptical (*E*). Their main geometry is shown in Fig. 2. The internal structure of the top layer is also varied by defining the high (*HD*) and low density (*LD*) chamber arrangements.

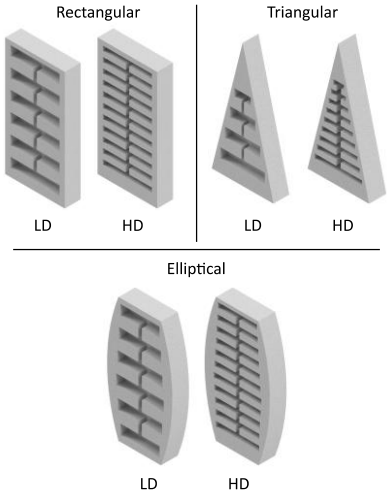

Fig. 2. Main types of soft actuators, illustrated with the perforated top parts

The actuator geometry is defined by a series of parameters, as shown in Fig. 3. To generate the desired actuator from the given input parameters, a Python script was used to calculate the geometric points and then generate the SVG files used to laser-cut the acrylic moulds. The components of an example mould are shown in Fig. 4. The mould is formed by glueing these parts together and securing them with bolts at the four corners.

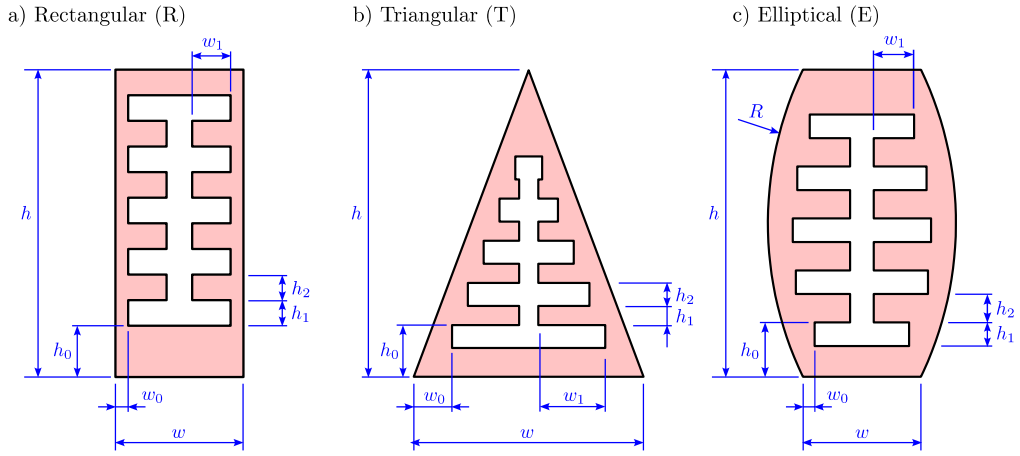

Fig. 3. The dimensions of the soft actuators

Fig. 4. Parts of the laser-cut acrylic mould for the rectangular soft actuator

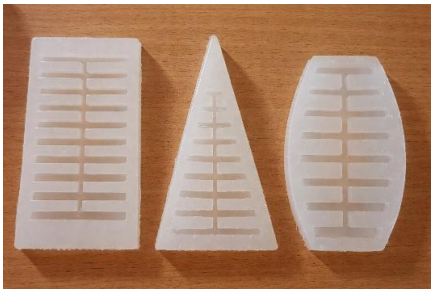

Fig. 5. The perforated top layers of the fabricated actuators

The fabrication process involved mixing the silicones with their catalyst at the ratio specified by the datasheets, then degassing the mixture in a vacuum chamber to remove air bubbles. This step ensures that the resultant silicone is homogeneous. The mixture was poured into the moulds and cured at room temperature for 24 hours. After curing, the silicone components were removed from the forms, resulting in the designated soft actuator geometries shown in Fig. 5. Residual stresses may develop during curing [22], but these effects are not considered in this work.

In total, 12 soft actuators are constructed using three geometries (*R, T, E*), two chamber arrangements (LD, HD) and two different materials in the top layer (*ECOFLEX* 00-30 and 00-50). The notation of the specimens will follow $G - D - M$, where G denotes the geometry (*R, T* or *E*), D denotes the chamber density (*LD* or HD) and M denoted the top layer material (*ELASTOSIL*, *ECOFLEX 00-30* or *ECOFLEX 00-50*). The general dimensions of the actuators are:

$$w \times h = 45mm \times 89mm, \tag{1}$$

while the specific geometric parameters are summarized in Table 1.

Table 1. Specific geometric parameters of all the fabricated actuators

Actuator shape	Chamber density	h_0 (mm)	h_1 (mm)	h_2 (mm)	w_0 (mm)	w_1 (mm)	R (mm)
Rectangle	Low	6.0	7.3	7.3	4.0	17.0	–
Triangle		15.7	7.0	7.0	5.9	14.4	–
Ellipse		4.0	7.4	7.4	1.3	12.6	126.0
Rectangle	High	6.0	3.8	3.8	4.0	17.0	–
Triangle		11.6	3.2	3.2	4.9	14.8	–
Ellipse		12.3	3.7	3.7	0.5	14.2	126.0

2.2. Material Characterization

As mentioned previously, three types of silicone materials are considered in this research. Their main properties are summarized in Table 2.

Table 2. Important properties of the used materials

Property	ECOFLEX 00-30	ECOFLEX 00-50	ELASTOSIL M 4601 A/B
Color	White translucent	White translucent	Reddish-brown
Density (g/cm³)	1.07	1.07	1.13
Shore hardness	Shore 00-30	Shore 00-50	Shore A-28
Mixing ratio (A:B)	1 : 1	1 : 1	9 : 1

To model the mechanical behaviour of the used silicone materials, a finite-strain, pure-elastic, isotropic behaviour is assumed for the silicone materials, which is widely applied to model the behaviour of soft pneumatic actuators. Hyperelastic constitutive models are derived from the strain energy function:

$$W = W(\boldsymbol{C}), \tag{1}$$

where:

$$C = \boldsymbol{F}^T\boldsymbol{F}, \tag{2}$$

is the right Cauchy-Green deformation tensor and F is the deformation gradient (and $\boldsymbol{F}^T$ denotes the transpose of $\boldsymbol{F}$) [23]. For isotropic materials the strain energy function can be written as:

$$W = W(\boldsymbol{C}) = \widetilde{W}(\lambda_1, \lambda_2, \lambda_3), \tag{3}$$

where λ_1, λ_2 and λ_3 are the principal stretches. The Cauchy stress tensor is calculated as:

$$\sigma = \frac{2}{J}\boldsymbol{F}\frac{\partial W(\boldsymbol{C})}{\partial \boldsymbol{C}}\boldsymbol{F}^T, \tag{4}$$

where:

$$J = \det(\boldsymbol{F}) = \lambda_1\lambda_2\lambda_3, \tag{5}$$

Is the volume ratio, for which holds $J \equiv 1$, assuming perfectly incompressible material behaviour [23].

The stress-strain characteristics of the silicone materials were determined by uniaxial tensile and compression tests using an *Instron 3345 Single Column Universal Testing System* equipped with an *Instron 2519-107* (5 kN) load cell. Multiple bone-shaped and cylindrical specimens were used, according to *ISO 37* and *ASTM D395* standards, as shown in Fig. 6.

The longitudinal stretches were captured by the testing system, while the transverse stretches were captured using the binarization image-processing technique applied to the video recordings, according to research recommendations [24, 25].

From the experimental data obtained, multiple fits were performed for incompressible hyperelastic material models, such as the neo-Hookean, Mooney-Rivlin, Yeoh, and Ogden models. From these, the third-order Ogden model provided the best fits for every material, which is written in the form as:

$$W(\lambda_1, \lambda_2, \lambda_3) = \sum_{i=1}^{3}\frac{2\mu_i}{a_i^2}\left(\lambda_1^{\alpha_i} + \lambda_2^{\alpha_i} + \lambda_3^{\alpha_i} - 3\right), \tag{6}$$

where μ_i and α_i are material parameters.

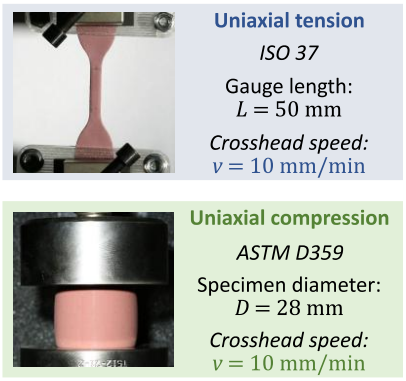

Fig. 6. Uniaxial tensile and compression tests were performed on the silicone specimens

The fits were obtained by minimizing the quality function:

$$Q = \sqrt{\frac{1}{M}\sum_{i=1}^{M}\left(\frac{P_i^{\mathrm{mod}} - P_i^{\mathrm{exp}}}{P_i^{\mathrm{exp}}}\right)^2} \tag{7}$$

where M is the number of data points, P_i^{mod} is the nominal stress given by the material model (using the uniaxial stress solution), and P_i^{exp} is the nominal stress acquired by the material tests. The produced fits can be seen in Fig. 7, where the coefficient of determination (R^2) is also provided, indicating the overall quality of the fit. The material testing results indicate (see Fig. 8) that the material behaviour can be assumed to be nearly incompressible $\nu \approx 0.5$, where the longitudinal and transversal stretches are related through:

$$\lambda_T = \lambda^{-\nu} \approx \lambda^{-0.5}. \tag{8}$$

The resulting hyperelastic material models were evaluated using the Drucker stability criterion to ensure their suitability for accurately capturing the nonlinear mechanical response of the actuators.

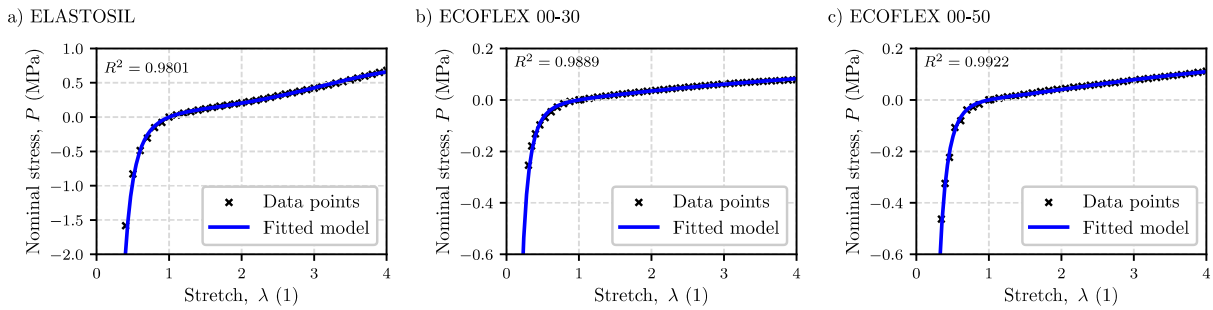

Fig. 7. The fitted third-order incompressible Ogden hyperelastic material models to experimental data

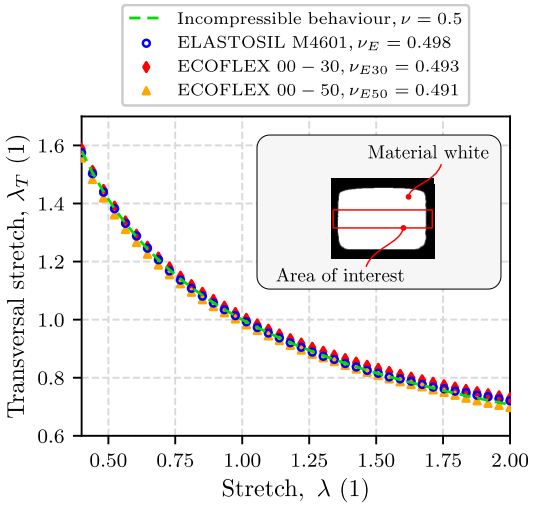

Fig. 8. Comparison of the longitudinal λ and the transversal (λ_T) stretch relation for the used silicone materials (the dashed green curve represents the theoretical relation for purely incompressible materials)

2.3. Numerical Simulations

Finite element simulations were performed in *ABAQUS 2024/Standard* to analyse the effects of geometric and material parameters. The simulations are developed through *Python* scripting, making it completely automatic.

The 3D geometric model (see Fig. 9) is constructed directly in *ABAQUS*, by sketch extrusions. The sketches are the result of connecting the geometric points calculated by the script, based on the given input geometric parameters.

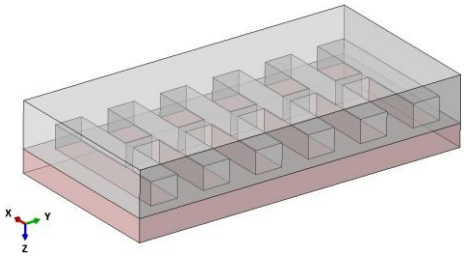

Fig. 9. The 3D geometric model of the rectangular actuator (the geometry is partitioned according to the bottom and top layers)

The geometry is partitioned according to the material assignments of the bottom and top layers. The discretization was performed with the built-in meshing algorithms, using 3D quadratic tetrahedron elements, with the hybrid formulation (C3D10H). The average mesh size was 2 mm. The mesh quality was verified by monitoring the element aspect ratio, which was kept below 55 to avoid excessive distortion, thereby ensuring reliable numerical accuracy. The generated mesh is shown in Fig. 10.

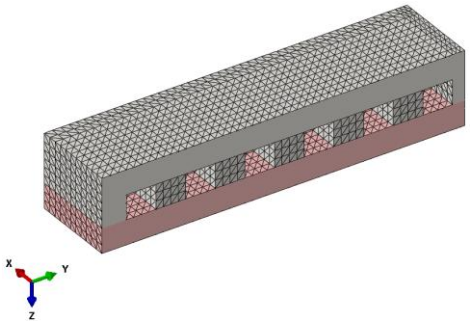

Fig. 10. The meshed finite element model of the rectangular actuator. The model is cut in half to represent the internal mesh

The solution is obtained in two static steps. In the first step, the effect of gravity is applied to the model (g equals 9.81 m/s^2 in the Z+ direction) to achieve the initial shape. The inflation starts from this deformed shape, which is driven by the fluid-cavity interaction, with an incompressible gas model. The cavity surface is the internal surface of the actuators, selected according to the analysed geometry. A reference point is established in the cavity to capture the volume and pressure of the stored fluid. The pressure of the cavity is raised in a linear way during the step, from the initial start equation of 0 kPa to 40 kPa. During both steps, the mechanical boundary conditions are imposed on the model to represent the fixture during testing. The defined interaction and the boundary conditions are shown in Fig. 11.

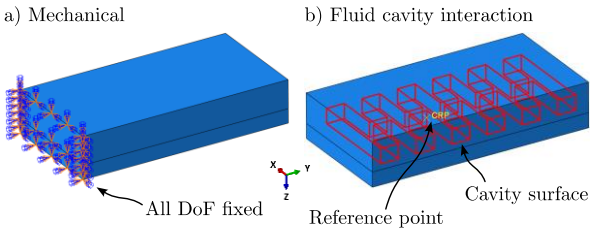

Fig. 11. The boundary conditions of the soft actuator

The numerical solution is obtained in a time period of 1 s, with the minimum, maximum and initial size of the time increment as 10^{-12} s, 10^{-2} s, 10^{-2} s, respectively. The maximum number of increments are set to 10000.

2.4. Experimental Testing

Experimental tests were performed to validate the results of the numerical simulations. The measurement setup consists of a self-developed fluidic control board, a fixture to hold the soft actuator, and a high-resolution camera to capture the bending motion. The setup is illustrated in Fig. 12.

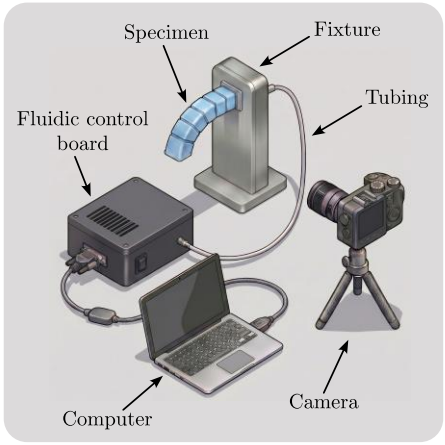

Fig. 12. Schematic diagram of the test setup

The fluidic control board supplies the required air pressure via a diaphragm pump, illustrated in Fig. 13. The setup is controlled by a microcontroller, which is also responsible for the data acquisition. An inline pressure sensor is responsible for getting an accurate reading of the current supplied pressure, while solenoid valves are responsible for controlling the air flow. The valves are controlled by *MOSFETs*, which are driven by PWM signals from the microcontroller. The control loop runs at a data rate of 400 Hz. The board is able to perform the pressurization by controlling the pump and the solenoid valves, such that the prescribed pressure is reached. Deflation is possible in the same way. To get accurate readings of the inline pressure sensor, the sensor is calibrated beforehand using known pressure sources.

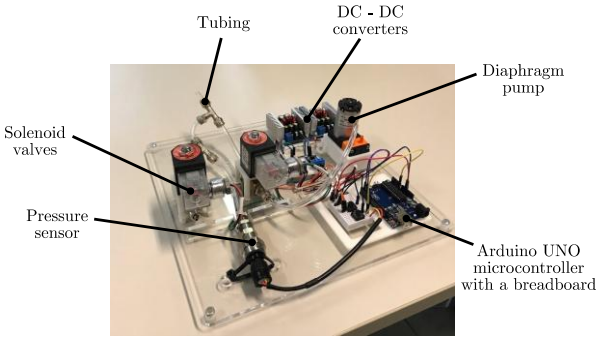

Fig. 13. The fluidic control board with it's components

The deformation of the soft actuator was monitored through the video recordings supplied by the camera. Image processing techniques using motion tracking were utilized in the Motion Tracker Beta software [26] to get the bending trajectory of the actuators. The trajectory (which can be seen in Fig. 14) is defined via the angle:

$$\theta(P) = \tan^{-1}\left(\frac{y(P)}{x(P)}\right), \tag{9}$$

where $x(P)$ and $y(\mathrm{P})$ is the result of the tracking between the origin O and the designated point on the trajectory P. The tracking is performed via the *CSRT* algorithm, and it is reconstructed as the vector:

$$\boldsymbol{\gamma}(\mathrm{P}) = [x(\mathrm{P}) \quad y(\mathrm{P})]^T. \tag{10}$$

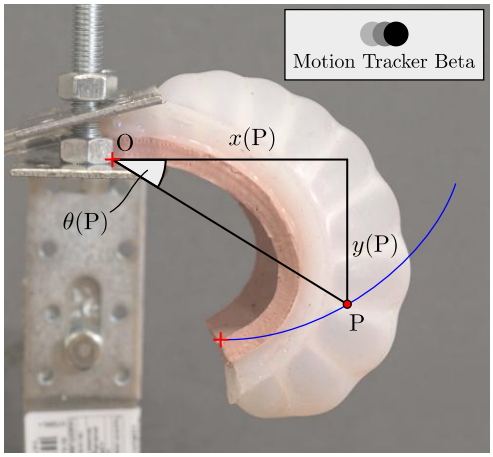

Fig. 14. Trajectory calculation from the video recording - the blue line represents the tracked trajectory, while the red markers represent the tracked points

The relation between the internal pressure p and the bending angle θ can be deduced, as both the fluidic control board and the tracked video recordings have the same timescale.

3. RESULTS AND DISCUSSION

The mechanical performance of the fabricated soft actuators was evaluated by comparing the numerical simulations from *ABAQUS*, with the measurement results obtained from the experimental testing.

3.1. Bending Trajectory and Angle Analysis

The bending trajectories obtained from the numerical simulations are summarized in Fig. 15. The results show that the trajectories are very close to each other, regardless of the main geometry type. This means that the actuators can be used in the same use case, as their ability to grip objects does not depend solely on the trajectory. Fig. 15a and Fig. 15c illustrate that the bending trajectories of the rectangular and elliptical actuators are more extended than the triangular actuator (see Fig. 15b), thereby expanding their capability to grasp larger objects.

However, the bending angle varies with respect to the used top layer material and chamber density. Fig. 16 shows that by using the *ECOFLEX* 00-30 as a top layer material, the acquired bending angle can be increased for the rectangular (Fig. 16a) and triangular (Fig. 16b) geometries. Interestingly, this does not happen for the elliptical (Fig. 16c) geometry. In this case, the higher chamber density yields a lower bending angle for the same internal pressure.

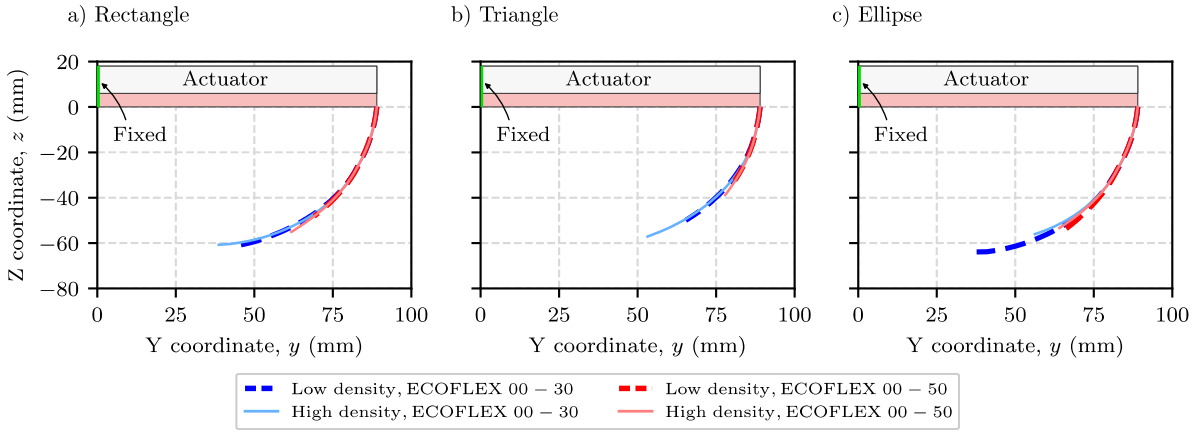

Fig. 15. The simulated bending trajectories of the actuators, for different materials and chamber density

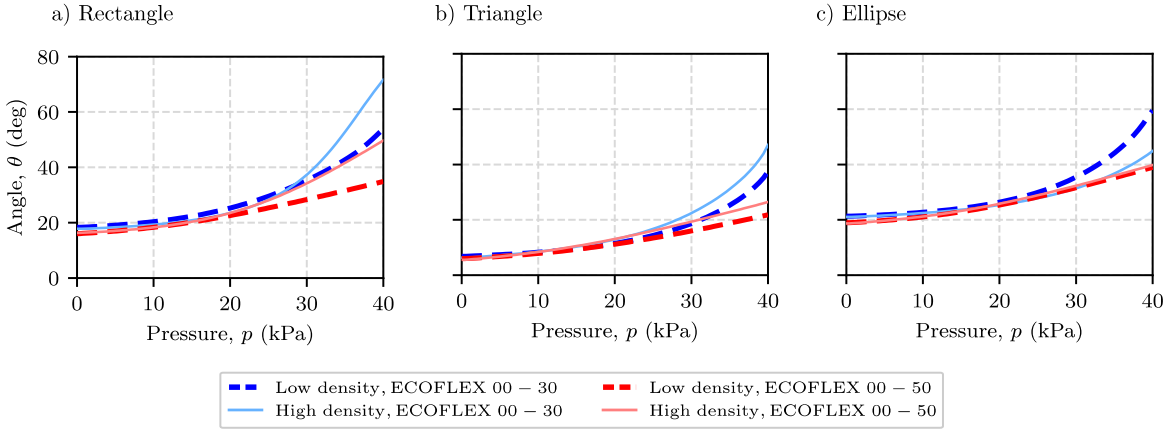

Fig. 16. The simulated bending angles of the actuators, for different materials and chamber density

The deformed shape for the elliptical actuator shows that the deformation of the top-layer walls is more prominent for the low-chamber-density model, as illustrated in Fig. 17, which results in significant asymmetry in the pressure distribution. This results in the low-chamber-density model bending more under the same internal pressure.

Fig. 16b indicates that the initial bending angle due to the gravitational load is comparatively smaller for the triangular actuator. This shows that, compared to the rectangular and elliptical geometries, the triangular design extends the actuator's functional range at low bending angles by an additional 12° . However, this advantage is balanced at higher pressures, where the rectangular and elliptical designs exhibit superior bending, eventually surpassing the bending angle of the triangular actuator.

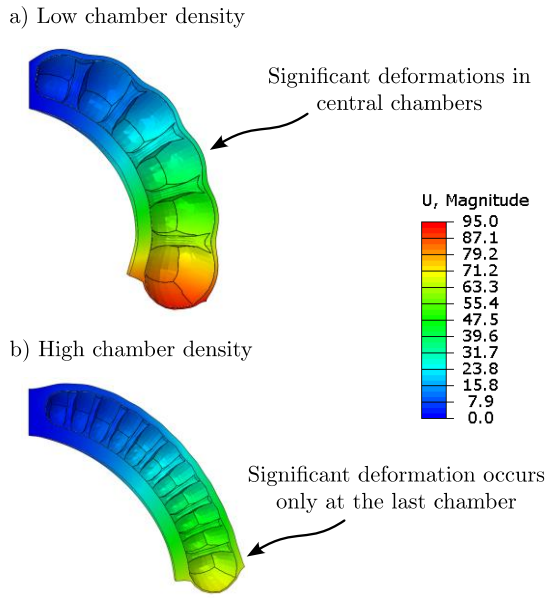

Fig. 17. Displacement maps of the ellipse geometry, with the ECOFLEX 00-30 top layer configuration

3.2. Experimental Validation of the Numerical Results

The validation of the numerical results in the first place is carried out by comparing the internal pressure – bending angle relation obtained by the numerical simulation and the experimental testing, shown in Fig. 18. The results indicate that the models accurately capture the bending states of the actuators relative to internal pressure, demonstrating a strong correlation between the simulated and physical behaviors.

As illustrated in Fig. 19, the comparison of the acquired trajectories further validates the predictive capabilities of the proposed framework, demonstrating strong agreement between the numerical and experimental results. The bending trajectory can be reconstructed using the simulation method with marginal error. Minor differences can be noticed at the last tracked and simulated point. The slightly greater length of the experimental trajectories suggests a minor temporal lag in the pneumatic system's response, where inflation continued briefly beyond the target pressure before stabilizing.

However, it is observed that the bending profiles of the triangular actuators exhibit a degree of variability; unlike simpler geometries, these specific designs are inherently more challenging to manufacture consistently, which can be seen on the deformed shape during experimental testing, depicted in Fig. 20b. This is primarily due to the intricate nature of their smaller geometric features, which are more sensitive to minor fabrication tolerances and material inconsistencies. Despite these manufacturing complexities, the model maintains a high level of fidelity in predicting the overall mechanical response. Fig. 20a and Fig. 20c shows that these intrinsic deformations are not present in the rectangular and elliptical actuators.

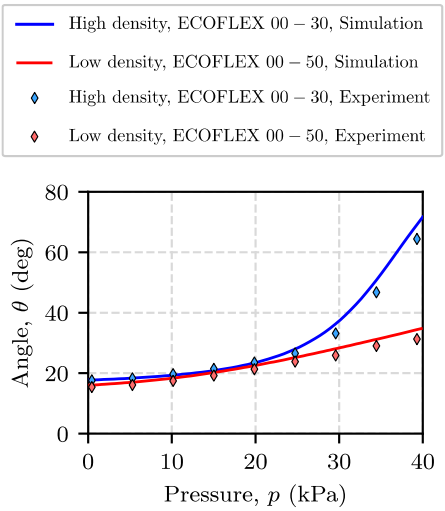

Fig. 18. Numerical and experimental bending angle results for the rectangular actuator

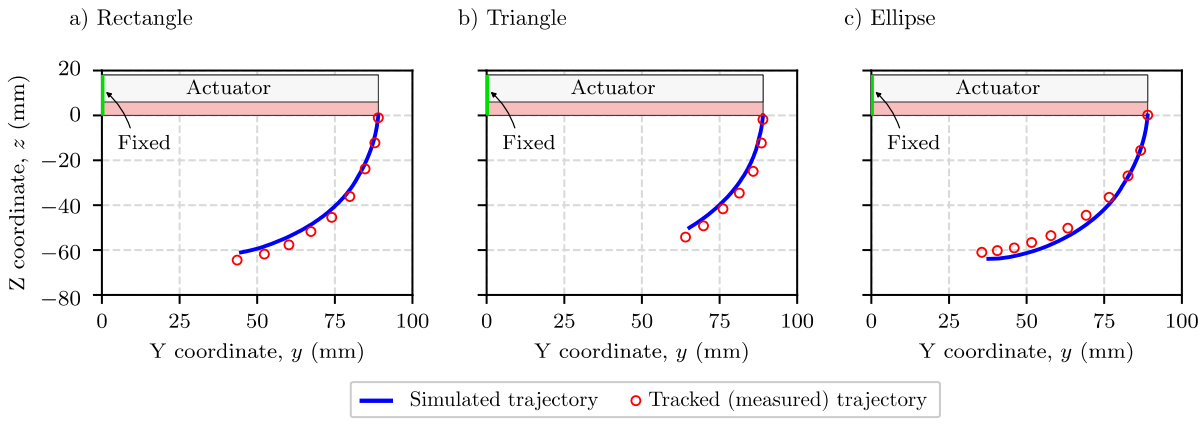

Fig. 19. The simulated and tracked bending trajectories for the *ECOFLEX* 00-30 top layer material and the low chamber density

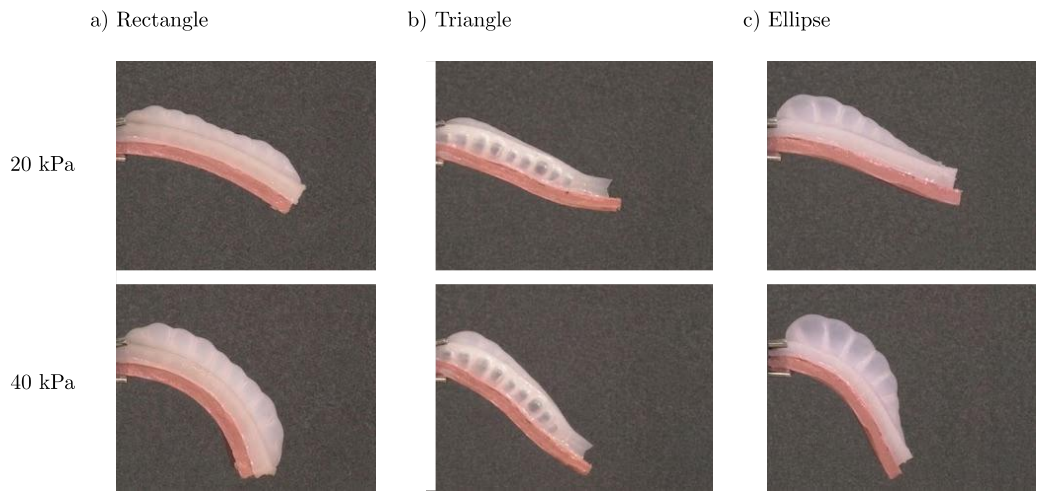

Fig. 20. Comparison of the deformed shape seen in experimental testing, at a selection of internal pressures, for different geometries and the *ECOFLEX* 00-30 top layer material

The experimental validation of the numerical models highlights that the simulation methodology – which is fully automated via the developed scripts – can be used to conduct parameter studies in both the geometric and material parameter spaces. The effect of different material combinations can lead to a variety of deformed shapes in a specified range of actuation pressures, making them suitable for a wide range of applications.

4. CONCLUSION

This work combined numerical simulations with experimental testing to investigate the behaviour of multi-material pneumatic soft actuators manufactured using laser-cut moulds. Hyperelastic material models were used together with parametric finite element simulations to evaluate how actuator geometry and material selection influence the bending performance.

The actuator shape was found to have a strong influence on the initial deflection. Among the tested geometries, the triangular actuator showed the smallest gravitational deflection at low pressures, allowing a larger usable bending range than the rectangular and elliptical designs. This makes the triangular geometry a promising option for applications requiring accurate motion at relatively low operating pressures.

At higher pressures, the rectangular and elliptical actuators produced greater bending forces, making them better suited for applications requiring higher grasping forces. Increasing the chamber density also improved the bending angle of the rectangular and triangular actuators. In contrast, the elliptical design showed little benefit from additional chambers because localized wall deformation and pressure asymmetry limited its performance.

Overall, the results demonstrate that actuator geometry and material selection have a major influence on performance and should be selected according to the intended application. The combination of numerical modelling and experimental validation presented in this work can support the design of soft actuators tailored to specific operational conditions.

NOTE

The shorter version of this research was presented at the *41st Danubia-Adria Symposium Advances in Experimental Mechanics*, held in Kragujevac, Serbia, on 23–26 September 2025.

ACKNOWLEDGEMENTS

The research has been supported by the Hungarian National Research, Development and Innovation Office, Hungary (NKFIH NKKP STARTING 149473) and by the János Bolyai Research Scholarship of the Hungarian Academy of Sciences, Hungary. The project, supported by the Doctoral Excellence Fellowship Programme (DCEP), is funded by the National Research Development and Innovation Fund of the Ministry of Culture and Innovation and by the Budapest University of Technology and Economics.

CONFLICT OF INTEREST

The authors declare no conflict of interest.

REFERENCES

[1] S. Hirai, R. Niiyama, T. Nakamura, T. Umedachi, T. Nakata, T. Tanaka. Soft Manipulation and Locomotion, In: K.

Suzumori, K. Fukuda, R. Niiyama, K. Nakajima (Eds.). *The Science of Soft Robots*. Springer, Singapore, 2023: 59-106. https://doi.org/10.1007/978-981-19-5174-9_4

[2] N. El-Atab, R.B. Mishra, F. Al-Modaf, L. Joharji, A.A. Alsharif, H. Alamoudi, M. Diaz, N. Qaiser, M.M. Hussain, Soft Actuators for Soft Robotic Applications: A Review. *Advanced Intelligent Systems*, 2(10), 2020: 2000128. https://doi.org/10.1002/aisy.202000128

[3] M.S. Xavier, C.D. Tawk, A. Zolfagharian, J. Pinskier, D. Howard, T. Young, J. Lai, S.M. Harrison, Y.K. Yong, M. Bodaghi, A.J. Fleming, Soft Pneumatic Actuators: A Review of Design, Fabrication, Modeling, Sensing, Control and Applications. *IEEE Access*, 10, 2022: 59442–59485. https://doi.org/10.1109/ACCESS.2022.3179589

[4] L. Gerez, C.-M. Chang, M. Liarokapis, Employing Pneumatic, Telescopic Actuators for the Development of Soft and Hybrid Robotic Grippers. *Frontiers in Robotics and AI*, 7, 2020: 601274. https://doi.org/10.3389/frobt.2020.601274

[5] Y. Jung, K. Kwon, J. Lee, S.H. Ko, Untethered soft actuators for soft standalone robotics. *Nature Communications*, 15(1), 2024: 3510. https://doi.org/10.1038/s41467-024-47639-0

[6] J. Shintake, V. Cacucciolo, D. Floreano, H. Shea, Soft Robotic Grippers. *Advanced Materials*, 30(29), 2018: 1707035. https://doi.org/10.1002/adma.201707035

[7] A. Sarker, T. Ul Islam, M.R. Islam, A Review on Recent Trends of Bioinspired Soft Robotics: Actuators, Control Methods, Materials Selection, Sensors, Challenges, and Future Prospects. *Advanced Intelligent Systems*, 7(3), 2025: 2400414. https://doi.org/10.1002/aisy.202400414

[8] L. Ge, L. Dong, D. Wang, Q. Ge, G. Gu, A digital light processing 3D printer for fast and high-precision fabrication of soft pneumatic actuators. *Sensors and Actuators A: Physical*, 273, 2018: 285–292. https://doi.org/10.1016/j.sna.2018.02.041

[9] A. Pal, V. Restrepo, D. Goswami, R.V. Martinez, Exploiting Mechanical Instabilities in Soft Robotics: Control, Sensing, and Actuation. *Advanced Materials*, 33(19), 2021: 2006939. https://doi.org/10.1002/adma.202006939

[10] Y. Chi, Y. Li, Y. Zhao, Y. Hong, Y. Tang, J. Yin, Bistable and Multistable Actuators for Soft Robots: Structures, Materials, and Functionalities. *Advanced Materials*, 34(19), 2022: 2110384. https://doi.org/10.1002/adma.202110384

[11] S. Zaidi, M. Maselli, C. Laschi, M. Cianchetti, Actuation Technologies for Soft Robot Grippers and Manipulators: A Review. *Current Robotics Reports*, 2(3), 2021: 355–369. https://doi.org/10.1007/s43154-021-00054-5

[12] M.H.O.R. Molla, J. Chen, C. Xu, Advancing soft robotics: recent progress in dielectric elastomer and fluid actuators. *npj Robotics*, 4, 2026: 17. https://doi.org/10.1038/s44182-026-00074-3

[13] P. Polygerinos, N. Correll, S.A. Morin, B. Mosadegh, C.D. Onal, K. Petersen, M. Cianchetti, M.T. Tolley, R.F. Shepherd, Soft Robotics: Review of Fluid-Driven Intrinsically Soft Devices; Manufacturing, Sensing, Control, and Applications in Human-Robot Interaction. *Advanced Engineering Materials*, 19(12), 2017: 1700016. https://doi.org/10.1002/adem.201700016

[14] X. Li, W. Wang, Z. Fang, P. Yan, H. Huang, B. Li, Rapid state-switching systems based on magnetic-actuated bistable 4R Mechanisms. *International Journal of Mechanical Sciences*, 321, 2026: 111661. https://doi.org/10.1016/j.ijmecsci.2026.111661

[15] M. Białek, D. Rybarczyk, Research on the operational properties of the soft gripper pads. *Scientific Reports*, 14, 2024: 32133. https://doi.org/10.1038/s41598-024-83956-6

[16] C. Zhang, H. Yang, R. Garziera, Y. Xu, H. Jiang, Reprogrammable gripper through pneumatic tunable bistable origami actuators. *International Journal of Mechanical Sciences*, 286, 2025: 109889. https://doi.org/10.1016/j.ijmecsci.2024.109889

[17] Z. Awada, Y. Haddab, M. Gouttefarde, PneuNet actuators design: Trade-offs between deformation, force, and resistance to buckling. *Sensors and Actuators A: Physical*, 386, 2025: 116307. https://doi.org/10.1016/j.sna.2025.116307

[18] K. Ruzsa, S. Berezvai, Experimental and Numerical Analysis of Laser-Cut Pneumatic Soft Robot Structures. In: *Proceedings of 41st Danubia-Adria Symposium Advances in Experimental Mechanics,* 23 - 26 September 2025, Kragujevac, Serbia, pp.45–46. https://doi.org/10.46793/41DAS2025.045R

[19] Abaqus/CAE 2024.HF8. *Dassault Systèmes Simulia Corp.*, Providence, RI, USA, 2024.

[20] Elastosil M 4601 A/B Datasheet. *Wacker Chemie AG.* (Accessed: 20 April 2026) https://www.wacker.com/h/enus/c/elastosil-m-4601-ab/p/000018458

[21] Ecoflex Series Datasheet. *Smooth-On*. (Accessed: 20 April 2026) https://www.smooth-on.com/tb/files/ECOFLEX_SERIES_TB.pdf

[22] S. Mukherjee, Influence of residual stress in failure of soft materials. *Mechanics Research Communications*, 123, 2022: 103903. https://doi.org/10.1016/j.mechrescom.2022.103903

[23] G.A. Holzapfel. Nonlinear solid mechanics: A continuum approach for engineering. *John Wiley & Sons*, Chichester, 2000.

[24] Y. Kwon, S.E. Seo, J. Lee, S. Berezvai, J. Read de Alaniz, C.D. Eisenbach, R.M. McMeeking, C.J. Hawker, M.T. Valentine, 3D-printed polymer foams maintain stiffness and energy dissipation under repeated loading. *Composites Communications*, 37, 2023: 101453. https://doi.org/10.1016/j.coco.2022.101453

[25] S. Berezvai, A. Kossa, Effect of the skin layer on the overall behavior of closed-cell polyethylene foam sheets. *Journal of Cellular Plastics*, 52(2), 2015: 215–229. https://doi.org/10.1177/0021955X15575801

[26] K. Floch, A. Kossa, Motion Tracker Beta: A GUI based open-source motion tracking application. *SoftwareX*, 23, 2023: 101424. https://doi.org/10.1016/j.softx.2023.101424